Journal of Solid Mechanics Vol. 9, No. 3 (2017) pp. 472-489

The Prediction of Forming Limit Diagram of Low Carbon Steel Sheets Using Adaptive Fuzzy Inference System Identifier

H. Aleyasin *

Department of Mechanical Engineering, Babol University of Technology, Babol, Iran

Received 28 May 2017; accepted 3 July 2017

ABSTRACT

The paper deals with devising the combination of fuzzy inference systems (FIS) and neural networks called the adaptive network fuzzy inference system (ANFIS) to determine the forming limit diagram (FLD). In this paper, FLDs are determined experimentally for two grades of low carbon steel sheets using out-of-plane (dome) formability test. The effect of different parameters such as work hardening exponent (n), anisotropy (r) and thickness on these diagrams were studied. The out-of-plane stretching test with hemispherical punch was simulated by finite element software Abaqus. The limit strains occurred with localized necking were specified by tracing the thickness strain and its first and second derivatives versus time at the thinnest element. In addition, to investigate the effect of different parameters such as work hardening exponent (n), anisotropy (r) and thickness on these diagrams, a machine learning algorithm is used to simulate a predictive framework. The method of learning algorithm uses the rudiments of neural computing through layering the FIS and using hybrid-learning optimization algorithm. In other words, for building the training database of ANFIS, the experimental work and finite element software Abaqus are used to obtain limit strains. Good agreement was achieved between the predicted data and the experimental results.

Keywords: Forming limit diagram; Out-of-plane; Localized necking; Finite element; Fuzzy inference system.

1 INTRODUCTION

THE sheet metal forming receives more and more application in the domains of automotive and aeronautics. Especially with the innovative techniques, such as hydroforming and incremental forming, the manufacture of complex parts with low tools cost can be realized. In metal forming technology, the formability of sheet is limited by localized necking or non-uniform strains that may occur within a small region in the sheet. The amount of strain that a sheet metal can tolerate just before localized necking is called limit strain. FLDs are plots of the major and minor principal strains which can be sustained by sheet materials prior to the onset of localized necking. The principal strain components at necking ($\varepsilon_1, \varepsilon_2$) are determined along the loading paths that range from uniaxial to biaxial, and a locus in strain space is obtained. This locus represents the limit of formability for the as-received sheet under monotonic or proportional loading paths. On this basis, the FLD is a useful measure to evaluate the formability of

*Corresponding author. Tel.: +98 9155840267.
E-mail address: h.aleyasin.2011@gmail.com (H. Aleyasin).

sheet metal. The most general realistic method was introduced at the beginning of the 1960s by Keeler and Backofen [1] and Goodwin [2] who proposed the concept of FLD.

The determination of FLDs is a complex task, and research on FLDs is still the subject of extensive experimental, theoretical and numerical studies. The experimental methods for determining FLDs are well established, stretching over a hemispherical punch [3] or a circular punch with a flat bottom in a Marciniak cup test [4]. In 1967, Marciniak and Kuczynski put forward a successful model to calculate limit strains in biaxial stretching region. The other test procedure is the conventional out-of-plane (dome) test where a sheet metal sample is clamped between circular die rings and is deformed by a hemispherical punch. A set of specimens with a fixed length, different widths and lubrication conditions were prepared following the method proposed by Hecker [3]. The out-of-plane formability test has been used more extensively than the Marciniak in-plane test. Raghavan [5] proposed a simple technique to prepare in-plane specimens for different strain states. By forming a number of sheet specimens with varying widths, different strain states were obtained. The specimens were deformed to fracture and the strain state was evaluated just outside the fracture zone by circle grid method or digital image correlation technique. Finally, by connecting all the limit strain points, the forming limit curve (FLC) was drawn. Experimental determination of a FLD is very time consuming and requires special equipments, which may not always be available.

Moreover, with increasing computational techniques, the numerical predictions of FLDs have become more attractive and the finite element method (FEM) has been selected to simulate the out-of-plane test. By means of FEM, the strains and the stresses in the elements of the sheet metal can be simultaneously calculated in a numerical simulation for each loading step. To analyze the simulation results for the onset of necking, it is essential to establish a failure criterion. To predict the FLD numerically, some procedures have been used for the definition of localized neck under various sheet metal forming conditions.

Many studies have suggested an approach to predict the forming limit by introducing criteria for ductile fracture into finite element simulation of sheet metal forming processes [6-9]. In this approach the forming limit is predicted not by the onset of localized necking but by the occurrence of fracture itself. In this criteria the occurrence of ductile fracture is estimated by the macroscopic stress and strain during forming, which are calculated by the finite element simulation.

Burn et al. [10] predicted the localization by introducing the idea of the second time derivative of the thickness strain. Using the same test, Geiger and Merklein [11] considered that the gradient of major strain changed rapidly when localized necking occurred. Petek et al. [12] and Pepelnjak et al. [13] introduced an alternative method in which the second time derivative of the thickness strain is related to the single node or element that defines the time and area of localized necking. They proposed that the maximum of the second temporal derivative of thickness strain corresponded to the onset of necking. In some recent literatures, efforts to investigate the prediction of localized thinning as a function of material anisotropy have been expanded (Friedman and Pan [14], Huang et al. [15], Cao et al. [16] and Wu et al. [17]).

Due to the complexity of the sheet metal forming process and inter relationships among the process variables (die design, equipment selection, preform design of blank profile, friction and lubrication), it is difficult to develop a practical model solution, especially in three-dimensional problems. Currently, soft computing techniques, such as fuzzy inference systems or artificial neural network have been good approaches to overcome this phenomenon. It has been proved that the neural network application has fine adjustments for the fuzzy model. In 1993, Jang [18] proposed the adaptive neural-fuzzy inference system (ANFIS). In this modeling method, a hybrid-learning procedure is used to adjust the membership function parameters based on a set of given input–output data. This adjustment allows the fuzzy system to learn from the modeling data.

Recently, the non-traditional approaches such as fuzzy logic and neural networks have been extensively utilized in modeling the metal forming processes. Lin and Tai have used neural networks to predict the springback in an L-shaped bending process [19]. Inamdar et al. [20] used the same method to predict the springback in an air V-bending process, and in a similar study, Kim et al. [21] predicted the ductile fracture and free boundary surface profile in various aspect ratios for the upsetting process. Cao et al. [22] indicated the exceptional ability of a neural network along with a stepped binder force trajectory to control springback angle and maximum principal strain in a simulated channel forming process. Kazan et al. [23] developed a predictive model of springback in wipe-bending by neural network, based on data obtained from finite element analysis. Wu et al. [24] employed the combination of polynomial networks and genetic algorithms to design the optimal shape of extrusion die. Fuzzy logic is used to control and predict different variables and parameters of the forming processes. Yang et al. [25] utilized the fuzzy inference model to predict the flow stress. Manabeet et al. [26] used a fuzzy model to control the blank-holder force in deep drawing of plates. Optimum bending and setting-up sequences in sheet metal forming by fuzzy inference were studied by Onget al. [27]. Baseri et al. [28] modeled the springback in V-die bending process by using fuzzy

learning back-propagation algorithm. Lu et al. [29] successfully built an inverse architecture for adaptive-network-based fuzzy inference system (ANFIS) to explore the preform shape in the sheet bore-expanding process. They also [30] successfully built an inverse architecture for ANFIS to study ductile fracture and the preform shape in the upsetting process.

As aforementioned, the FLD is a useful diagnostic tool for trouble shooting in sheet metal forming operations and is also an assessment method for determining the formability of different sheet materials. In the present work, after studying the forming limit diagram of two low carbon steel sheets experimentally and numerically and evaluating the limit strains, the integrated learning database is served for ANFIS to predict the FLDs. The hybrid-learning algorithm is applied in ANFIS to be efficiently trained, and the impact of bell-shape membership function is found. The results of ANFIS in comparison with experimental work and numerical simulation are assessed. Meanwhile, in order to determine the FLD a numerical finite element simulation of the out-of-plane test is carried out and the obtained results are compared with those from the experiment. Although this investigation proves that ANFIS is a useful optimal soft computing approach in the sheet metal forming category, obtaining accurate training data for ANFIS is not always a simple task.

2 EXPERIMENTAL WORK

2.1 Material and equipment

As a verification of the ANFIS and finite element simulation, experiments are organized on hydraulic press of capacity 500 *kN* for stretching process. In this study, the low carbon steel sheets contain ST14 with thickness of 0.7 *mm* and ST12 with thicknesses of 0.7 *mm*, 1 *mm* and 1.25 *mm* are utilized for the experiments. At first, the mechanical properties of steel sheets are obtained in uniaxial tension tests along different directions by tensile testing machine (Instron) with a maximum tensile force capacity of 5 *kN*.

Table 1
Mechanical and formability properties of the materials at $0^{\circ}, 45^{\circ}$ and 90° from rolling direction.

	Tensile direction	Yield strength (*MPa*) (0.2%)	Ultimate tensile strength (*MPa*)	Total elongation(%)	Anisotropy (*r*)	Strain hardening coefficient (*n*)	$n \times r$
ST12	0	182	312	38	1.73	0.217	0.375
	45	190	318	37	1.54	0.201	0.309
	90	185	319	37	1.88	0.209	0.392
	Average	185.66	316.33	37.33	1.67	0.209	0.346
ST14	0	145	300	42	1.87	0.233	0.435
	45	158	307	36	1.65	0.221	0.364
	90	154	297	40	2.14	0.232	0.496
	Average	152.33	301.33	39.33	1.82	0.228	0.414

The standard tensile properties namely, 0.2% yield stress (YS), ultimate tensile stress (UTS), total elongation, strain hardening exponent (*n*) and the plastic strain ratio (*r*) are determined from the load–elongation data obtained from these tests and shown in Table 1. A constant cross head speed of 0.5 *mm*. min^{-1} is employed in all cases. The normal anisotropy ($\bar{r}$) is calculated using following equation.

$$\bar{r} = \frac{r_o + 2r_{45} + r_{90}}{4} \tag{1}$$

2.2 Test procedure

In this work, various strain states, including negative and positive minor strain ratios, are generated using Hecker simplified technique. The out-of-plane test tooling is used for obtaining limiting strains, Fig. 1. The out-of-plane test is carried out with single action hydraulic press of capacity 500 *kN* with 102 *mm* diameter hemispherical punch at constant punch velocity of 5 *mm*. min^{-1}. All possible strain states in the left and right-hand sides of an experimental FLD are obtained by stretching eight samples with widths changing from 25 to 200 *mm* in the length of 200 *mm*. Fig. 2 shows the specimens for out-of-plane stretching test. The blanks with the widths of 25, 50, 75 and 100 *mm* have an hourglass shape, which is required for narrow blanks to prevent failure occurred at the blank-holder. In this

method, the experimental procedure mainly consists of three stages: grid marking of the sheet specimens, punch-stretching of samples to failure (or onset of localized necking) and measurement of strains.

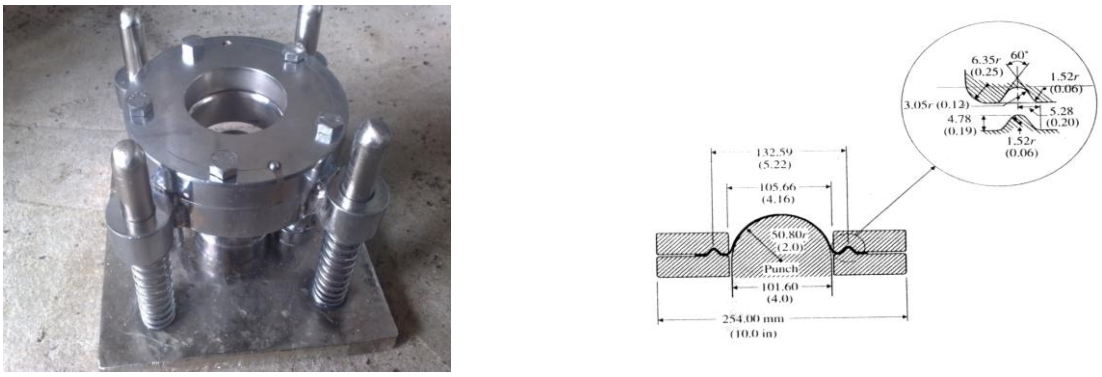

Fig.1
Schematic diagram for tooling geometry and the dimensions of the out-of-plane FLD tests.

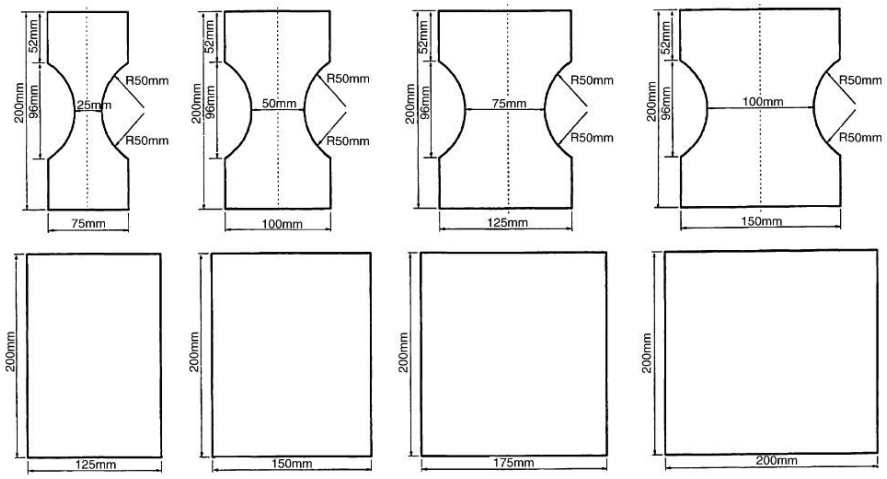

Fig.2
The specimens for out-of-plane stretching test.

2.2.1 Applying circle grids to the blanks

A circle-grid pattern with a diameter of 2.5 *mm* is electro-chemically etched on the surface of all specimens.

2.2.2 Punch-stretching the grid-marked samples

The test specimens are clamped between the upper and lower dies through closing the five bolts and the specimens are pushed on the die surface by blank-holder force. To prevent from any drawing-in during testing of sheet, a binder force of 100 *kN* is applied. Samples are formed up to fracture using a single action hydraulic press of capacity 500 *kN* with standard die and punch set up. A schematic view of die and press is shown in Fig. 3. The specimens are deformed until the first crack initiated on the sample, which can be seen visually or directly from the display of punch force on the force gage of hydraulic press. For each blank width, at least three specimens are tested to obtain more data points. Fig. 4 shows the failure positions in the tested specimens.

2.2.3 Measuring strains from deformed circles

The sheet samples are subjected to different states of strain namely tension–tension, plane strain and tension-compression by varying the width of the samples. During forming, the grid circles are deformed to elliptic shapes with different sizes because of stretching strain that is inserted in the plane of the sheet metal. For each specimen the major and minor limited strains are measured from the major and minor axes of the ellipse that is located at around regions of visible necking and fracture with an accuracy of 0.01 *mm* using a megapixel camera while the camera is exactly placed vertically and straight in front of the crack of the specimen, Fig. 5. Major and minor strains, e_1 , e_2, are calculated in three distinct regions namely safe, necked and fractured regions for all blanks. Finally, the empirical FLDs are drawn by plotting the minor strain along the abscissa and the corresponding major strain along the ordinate. A curve which separates the safe from the unsafe regions can now be drawn, Fig. 6.

Fig.3
A schematic view of the die and hydraulic press.

Fig.4
Sample stamped specimens used for FLD determination with fracture after testing.

Fig.5
Strain measurement equipment.

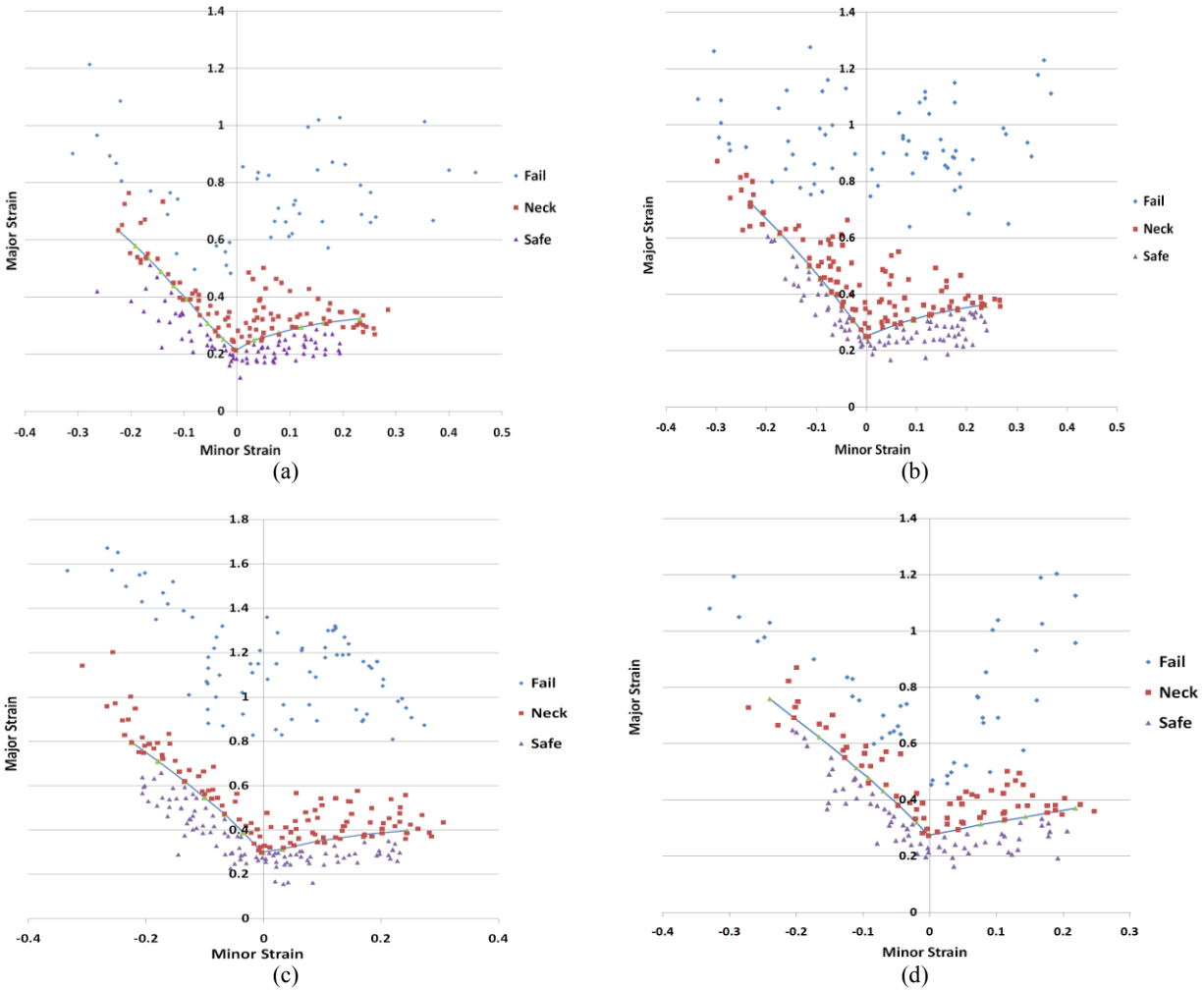

Fig.6
The experimental FLDs for sample sheets: (a) St12-0.7 *mm*, (b) St12-1 *mm*, (c) St12-1.25 *mm*, (d) St14- 0.7 *mm*.

3 FINITE ELEMENT SIMULATION

The finite element software Abaqus is used to simulate out-of-plane stretching test to determine the forming limit of sheet metals. The results are adopted to establish the database for ANFIS. The FE model for the out-of-plane test is composed of a rigid hemispherical punch, an upper die, a lower die with draw bead and a deformable sheet, Fig. 1. A quarter of model is built due to the symmetrical condition. The S4R element is used in the mesh module. In order to capture the strain localization, the mesh must be sufficiently small and regular. To increase the accuracy, the mesh size in the contact area under the punch is finer than the other parts. Fig. 7 shows one-quarter of simulation model with a diameter of hemispherical punch as 100 *mm*. The material is modeled as elastic–plastic where the elasticity is taken to be isotropic and the plasticity is assumed as both isotropic and anisotropic conditions. The elasticity of the specimen is defined with a Young modulus 200 *GPa* and a Poisson ratio of 0.3. The anisotropic properties are described by the Hill quadratic yield criterion.

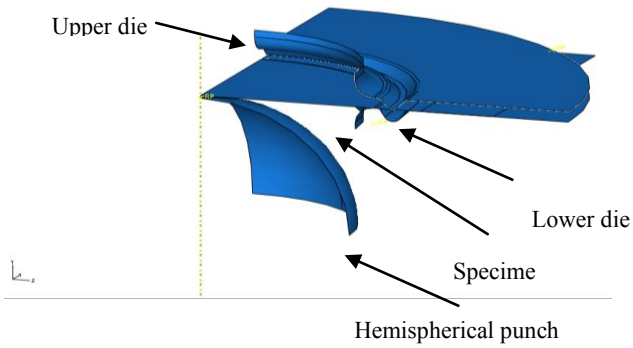

Fig.7
FE model of out-of-plane test.

The contact interaction is modeled by coulomb law, i.e. the friction coefficients for the punch-blank and die-blank are taken as 0.16 and 0.05, respectively. To take care of the convergence problem, the explicit solver is used. Because of in the explicit solver the stability condition is checked for the assurance of the real converged values, the internal energy and kinetic energy curves are presented to prove it as shown in Fig. 8. The simulation process is performed in two steps. In the first step, the upper die moves down in the *y*-direction and deforms the sheet into drawbead with a 100 *kN* force to prevent the specimen sliding between the upper die and the lower die. The hemispherical punch and the lower die stays fixed during this step. In the second step, while the boundary conditions from the first step are still in effect, the punch started to move up in the y-direction until the desired displacement is achieved.

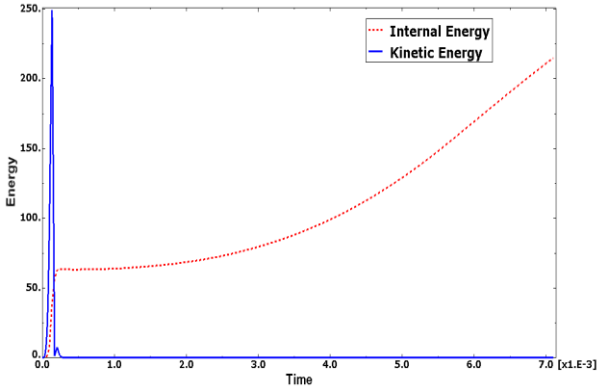

Fig.8
Internal energy and kinetic energy as a function of time for blank *st*12, thickness 1 *mm* and 200*100 *mm*.

The yield criterion of Hill is adopted [31] which can be expressed as:

$$f(\sigma)=\sqrt{F(\sigma_{22}-\sigma_{33})^2+G(\sigma_{33}-\sigma_{11})^2+H(\sigma_{11}-\sigma_{22})^2+2l\sigma_{13}{}^2+2M\sigma_{31}{}^2+2N\sigma_{12}{}^2} \quad (2)$$

where σ_{ij} denotes the stress components and F, G, H, L, M and N are material constants obtained by tensile tests of the material in the different directions. These constants can be expressed in terms of six yield stress ratios R_{11}, R_{22}, R_{33}, R_{12}, R_{13} and R_{23} according to following relations:

$$\begin{cases} F=\frac{1}{2}\left(\frac{1}{R_{22}^2}+\frac{1}{R_{33}^2}+\frac{1}{R_{11}^2}\right) \\ G=\frac{1}{2}\left(\frac{1}{R_{33}^2}+\frac{1}{R_{11}^2}-\frac{1}{R_{22}^2}\right) \\ H=\frac{1}{2}\left(\frac{1}{R_{11}^2}+\frac{1}{R_{22}^2}-\frac{1}{R_{33}^2}\right) \\ L=\frac{3}{2R_{23}^2}\quad , \qquad M=\frac{3}{2R_{31}^2}\quad , \qquad L=\frac{3}{2R_{12}^2} \end{cases} \quad (3)$$

The anisotropic material data are defined as:

$$\begin{cases} R_{11} = R_{13} = R_{23} = 1 \\ R_{22} = \sqrt{\dfrac{R_{90}(R_0+1)}{R_0(R_{90}+1)}} \\ R_{33} = \sqrt{\dfrac{R_{90}(R_0+1)}{R_0+R_{90}}} \\ R_{12} = \sqrt{\dfrac{3(R_0+1)R_{90}}{2(R_{45}+1)(R_0+R_{90})}} \end{cases} \tag{4}$$

where R_0, R_{45} and R_{90} are the plastic strain ratios in different directions relative to the rolling direction, Table 1.

Fig. 9 shows the effective plastic strains distribution obtained from the finite element simulation of the out-of-plane stretching test at the onset of necking. It shows the location or elements in which the specimen thickness is the thinnest. As it can be seen the strain localization zones are clearly visible; however, the evaluation of the limit strains is not completely unambiguous.

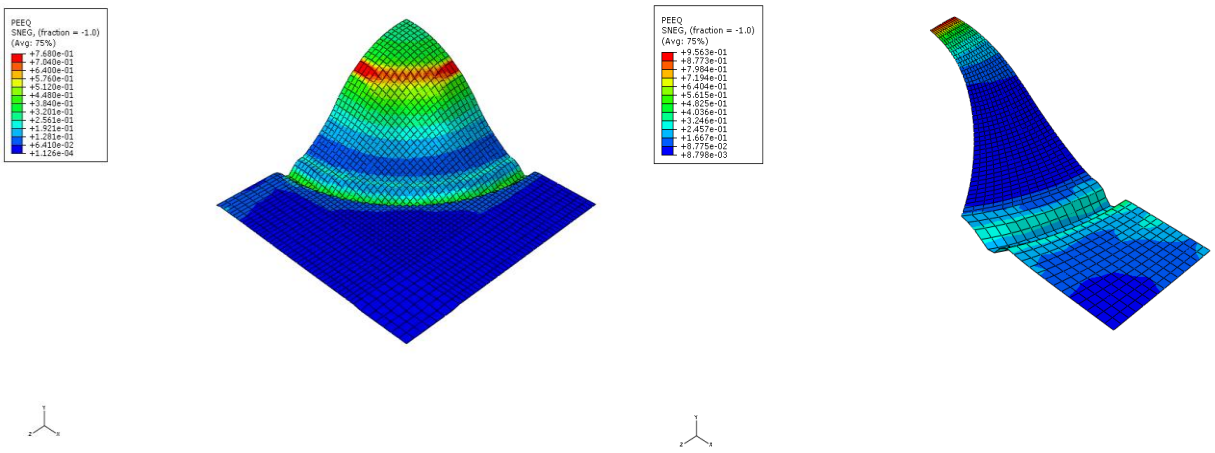

Fig.9
Plastic strain distribution of the square and notched specimens.

According to Petek et al. [12] and Pepelnjak et al. [13] methodology, the localized necking is specified by tracing the thickness strain and its first and second derivatives versus time at the thinnest node. Fig. 10 shows the thickness strain versus deformation time and its derivatives for a particular element. As can be seen, when necking appears, a sharp change in the strain behavior of the selected element occurs and a knee can be observed on the curve. Thus, considering the thickness strain rate versus time, the first temporal derivative of strain reaches its maximum. Moreover, the second derivative of thickness strain versus time represents a peak which shows the onset of necking in the specimen, Fig. 10. The limit strains are determined by evaluating the main strain states for the selected node at the onset of necking. To obtain the points of strain based FLC, different specimen geometries are simulated and the main strain states are analyzed for the critical nodes, according to the procedure described above. Fig.11 shows the FLDs obtained from the numerical simulation for the low carbon steel sheet (ST14) with the thickness of 0.7 *mm* and the low carbon steel sheet (ST12) with the thicknesses of 0.7 *mm*, 1 *mm* and 1.25 *mm*. The predicted FLDs are compared with the experimental data. In addition to the results indicated in the Fig. 11, the simulated FLDs for ST14 with two thicknesses of 1 *mm* and 1.25 *mm* in the isotropic and anisotropic conditions are obtained, Fig. 12.

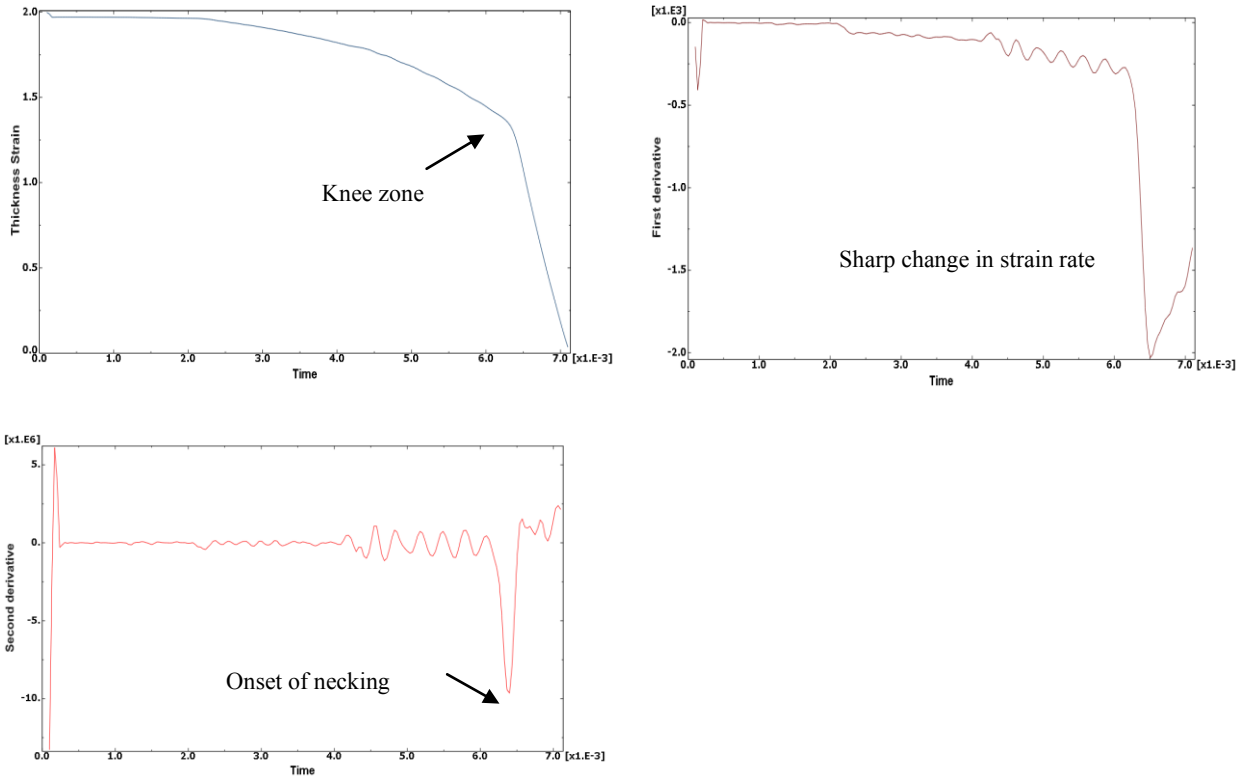

Fig.10
Thickness strain as a function of time and its derivatives for a particular specimen.

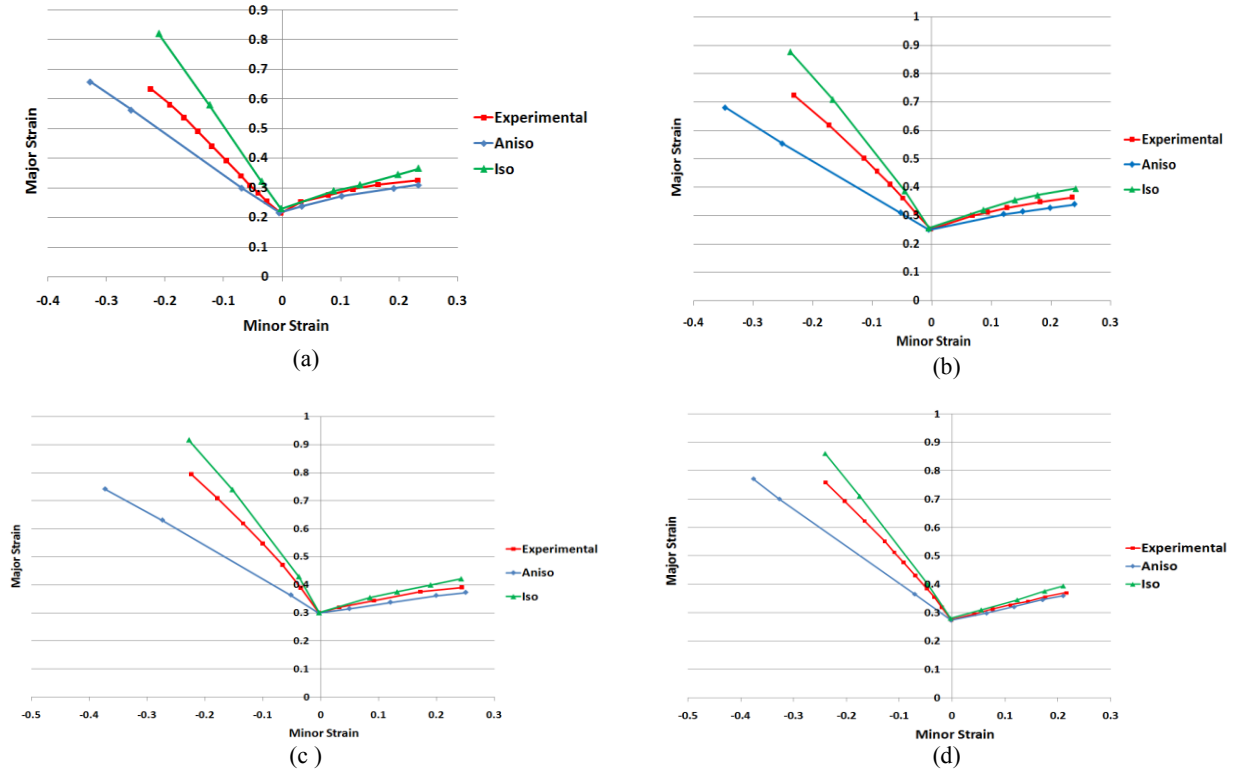

Fig.11
The experimental and numerical FLDs (a): St12-0.7 *mm*, (b) St12-1 *mm*, (c) St12-1.25 *mm*, (d) St14- 0.7 *mm*.

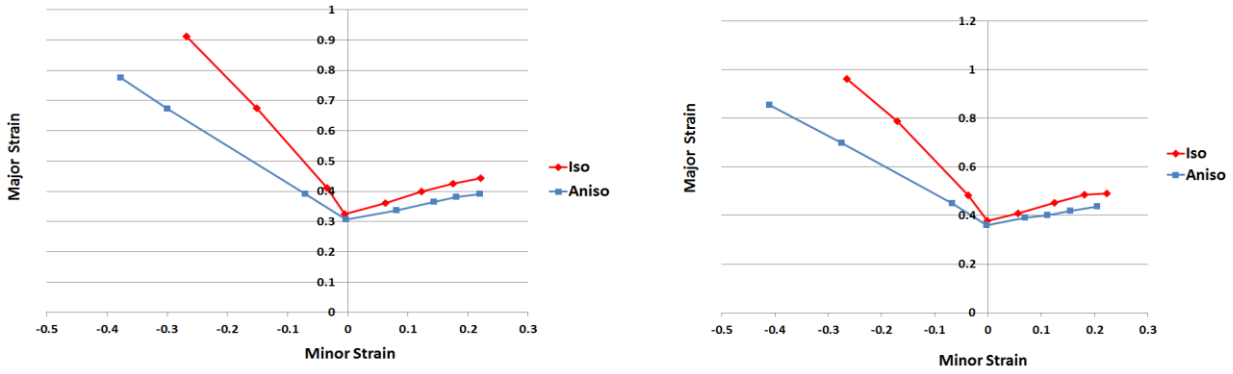

(a) (b)

Fig.12
The numerical FLDs:(a) St14-1 *mm*, (b) St14-1.25 *mm*.

4 NEURO_FUZZY INFERENCE SYSTEM

Adaptive neuro-fuzzy inference system (ANFIS) is constructed based on the concept of developing a FIS using neuro computing methodologies, i.e. multi layered architecture and back propagation learning approach. Let the input and output vectors of Takagi-Sugeno-Kang Fuzzy Inference (TSK-FIS) be defined as $x = [x_1, x_2, ..., x_r] \in R$ and $y_k = [y_1]^T \in R$ respectively where r represents the number of input parameters required for system identification. The obligation of ANFIS is to generate a map between input and output features. The rules of ANFIS are of TSK type as given in below:

$$R_m^{(i)} : IF x_1 is A_{i_1}^{(r)} AND .. AND x_r is A_{i_r}^{(r)} THEN\ y_1^{(i)} = g_1^{(i)} \tag{5}$$

The architecture of ANFIS includes 5 different layers. Number of nodes in layer one is related to the number of inputs and the number of membership functions (K_i) for each input. Number of nodes in layers 2-4 depends on the number of rules (R) in the fuzzy rule base. The steps required to construct each layer of the ANFIS are explained in below.

Step 1

The first layer is known as fuzzification layer. The input $X_i(p)$ is transformed to linguistic labels A_{ij} that represents the membership grade of fuzzy set. The node function of this layer can be defined as:

$$O_{ij}^1 = \mu_{ij}\left(X_i(p)\right), \qquad i = 1,...,r; j = 1,...,K_i \tag{6}$$

where μ_{ij} represents the j^{th} membership function for the input X_i (p) and O_{ij}^1 is the output of node ij. The membership function usually adopts bell-shape with maximum and minimum equal to 1 and 0, respectively as:

$$\mu_{ij} = \frac{1}{1 + \left| \frac{x - c_i}{a_i} \right|^{2b_i}} \tag{7}$$

where $\{a_i\ b_i\ c_i\}$ represents the parameter set. It is significant that if the values of this parameter set change, the bell-shape function will change accordingly. Meanwhile, the membership functions are also different in linguistic label A_{ij}. The parameters in this layer are named as premise parameters.

Step 2

The second layer is known as product layer. The output of each node (k) at this layer is a product of incoming inputs.

$$O_k^2 = \prod_{j=1}^{r} \mu_{ij}^{(i)} = \left(x_j\right) \tag{8}$$

Step 3

The third layer is known as normalized layer. The k^{th} node determines the ratio of k^{th} rule's firing strength to the sum of all rule's firing strengths.

$$O_k^3 = \bar{\mu}_i\left(x\left(p\right)\right) = \frac{\mu_i\left(x\left(p\right)\right)}{\sum_{i=1}^{R}\left(x\left(p\right)\right)} \tag{9}$$

Step 4

The next layer is known as defuzzification layer. Each node in this layer yields the weighted output of the TSK-type FIS as below

$$O_k^4 = w_k O_k^3 \tag{10}$$

where w_k represents the output of k^{th} TSK-FIS rule as:

$$w_k = \sum_{i=1}^{r} p_i + r_k \tag{11}$$

where $\left(p_i, r_k\right)$ is the parameter set. The parameters in this layer will be referred as consequent parameters.

Step 5

The last layer is known as output layer in ANFIS structure.

$$O_k^5 = y_\circ\left(p\right) = \sum_{i=1}^{R} \bar{\mu}\left(x\left(p\right)\right) w_k \tag{12}$$

Based on this characteristic, the node outputs go forward till layer 4. The consequent parameters can be identified by the least square method in the forward learning. On the other hand, the error signal goes backward till layer 1; and the premise parameters can be updated by the descent gradient method in the backward learning. This learning procedure is referred as hybrid-learning. The merit of hybrid-learning procedure is that it can efficiently obtain the optimal premise parameters and consequent parameters in the learning process. The schematic of ANFIS architecture is indicated in Fig. 13.

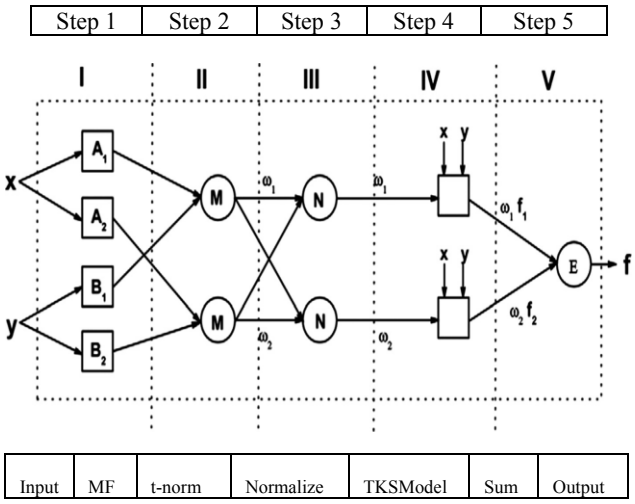

Fig.13
The architecture of ANFIS.

5 RESULTS AND DISCUSSION

5.1 Influence of r and n values

A comparison between the experimental forming limit curves for ST12 and ST14 steel sheets with thickness of 0.7 *mm* are shown in Fig. 14. In general, the strain-hardening exponent and the plastic strain ratio of a material can be considered as the most important parameters effect on the FLD. According to Fig. 14, the forming limit curve for ST14 steel sheet has more limiting strains than ST12. By increasing the strain-hardening exponent, the forming limit curves are shifted upward. The strain-hardening exponent generally delays the onset of instability until the higher strain value is reached.

The plastic anisotropy rises due to the preferred orientation of grains in a polycrystalline material which is usually characterized by the r value. It is usually known that the high plastic stain ratio or normal anisotropy is useful to improve the draw-ability (tension-compression strain condition), because it causes good resistance to thinning in the thickness direction during deep drawing. In the current study, the ST14 steel sheet has higher value of normal anisotropy, $\bar{r}$, than ST12 steel sheet, see Table 1. This means that ST14 steel sheet of thickness 0.7 *mm* shows higher draw-ability than ST12 with the same thickness. According to Fig. 14, the difference between the FLDs in the tension-tension strain condition (stretch ability) is less than that of the tension-compression part.

In other words, the effect of normal anisotropy in the left-hand side is more than that in the right-hand side which verifies what is known as the better formability of the tension–compression region. Furthermore, the average value of $n \times r$ represents the stretch-ability of a material so that the higher amount of $n \times r$ shows more stretch-ability [32]. Table 1. shows that the average value of $n \times r$ for ST14 steel sheet is more than that of the ST12 which shows the better stretch-ability of ST14 steel for the same thickness, Fig. 14.

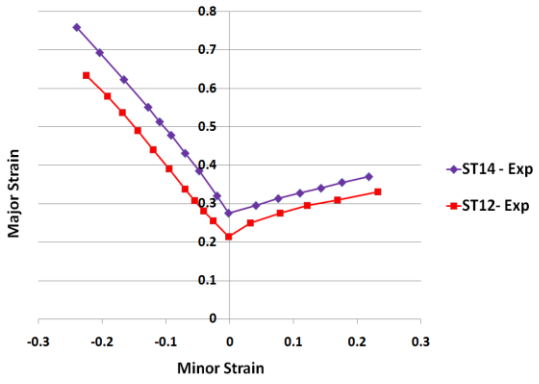

Fig.14
The experimental forming limit curves of St12 and St14 steel sheets with thickness of 0.7 *mm*.

5.2 Influence of sheet thickness

It is commonly believed that the thickness of sheet metal has a strong influence on its formability. Fig. 15 shows the different FLDs obtained from the experimental results for the low carbon steel sheets ST12 with three thicknesses of 0.7 *mm*, 1*mm* and 1.25 *mm*. It is visible that the steel sheet of thickness 1.25 *mm* exhibits better stretch-ability and draw-ability than that of other two thicknesses. Other authors have also confirmed the effect of thickness on sheet formability. For instance, based on the experimental and numerical calculations of Triantafyllidis and Samanta [33] were predicted that there is no significant difference between the strain corresponding to the onset of localization and the fracture strain for thin sheets. For thick sheets, however, they predicted that strain localization did not proceed rapidly after the onset of localization. Therefore, they demonstrated that increase in forming limits with sheet thickness has a higher nearby failure rather than the onset of localization. Moreover, Jenabali Jahromi et al. [34] illustrated the role of thickness on the low carbon steel sheets that the increasing thickness has positive effect on the formability.

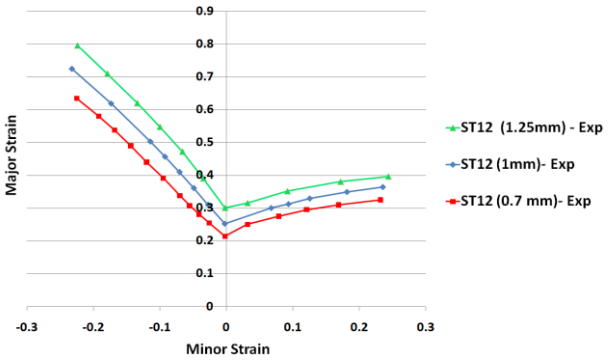

Fig.15
Effect of thickness on the FLD of St12 steel sheet.

By comparing the obtained results, it can be concluded that the effect of strain-hardening exponent and plastic anisotropy are more significant than thickness in increasing the formability, i.e. the FLD of ST14 with higher strain-hardening exponent and plastic anisotropy than ST12, is between the FLDs for ST12 with thickness of 1*mm* and 1.25 *mm*.

5.3 Prediction of limit strain by FE simulation

The results obtained from the FE simulation using Abaqus software are in good agreement with the experimental data, Fig. 11. The Exp, Iso and Aniso stand for the experimental and modeling data for isotropic and anisotropic conditions, respectively. Totally, in isotropic condition, the FLDs determined at the right- and left-hand sides have higher values of limit major strains than the experimental FLDs but the anisotropic simulated curves are under the experimental curves. This shows that in the equal strain-hardening exponent, the isotropic condition exhibit better formability than the anisotropic condition.

For both isotropic and anisotropic conditions, on the right-hand side, the obtained forming limit curves from numerical simulations are in consistent with the experimental results. However, the simulated curves for isotropic state have more tendencies toward experimental curves. On the right-hand side, the anisotropic curve of ST14 sheet with thickness of 0.7 *mm* has the best fit with the experimental results, Fig. 11(d). The isotropic curves have higher draw-ability than anisotropic and experimental ones, while the experimental data are placed between them.

In the anisotropic state, on the left-hand side of FLDs, with decreasing thickness the simulation curves approach to the experimental curves. But for the isotropic conditions, with increasing the thickness of the sheet, the slope of the simulation curves decrease and the curves approach the experimental curves. Therefore, the anisotropic simulated curves have lower values of the major strains than the experimental curves which show their more reliability for the practical application.

Another effective parameter in the forming limit curve is the principal strain known as FLD_O, which is equal to the major principal strain at failure when the minor principal strain is zero. According to Fig. 11, the forming limit strains in the plain-strain state, FLD_O are predicted by both isotropic and anisotropic conditions are in good agreement with the experimental results for all sheets. The values of FLD_O for the ST14 and ST12 sheets with the same thickness of 0.7 *mm* are 0.414 and 0.346, respectively. This increasing of FLD_O between these cases can be attributed to the effect of $n \times r$.

5.4 Prediction of limit strain by numerical study

Based on experimental and finite element works, the numerical study is performed to ascertain the veracity of the proposed technique for estimating FLDs of low carbon sheets. As mentioned, the aim of the experiments and numerical simulationsis determined whether the fuzzy logic programming can be useful for the current case study and on the other hand, the efficacy and accuracy of adaptive-network-based fuzzy inference system (ANFIS) technique for the forming problem is assayed.

Based on the obtained experimental data, the proposed models are trained. The input processing parameters include minor strain (ε_1) and thickness (t) and the output process parameter is major strain (ε_2) to obtain training data for ANFIS. Definition of proper fuzzy membership functions and the appropriate number of required rules are two major steps in applying ANFIS. To find the efficient structure of ANFIS, several networks with different membership functions are designed. To train these networks two stopping criteria are set. These criteria are error goal of zero and number of 20 epochs. In other words, the training process stops whenever the designated epoch number is reached 20 or the training error goal is achieved zero.

After checking all of the designed ANFISs, the network that revealed optimum accuracy in anticipation of test data is selected. The bell-shape membership function is adopted in the ANFIS training. After seeking various number membership functions, the best number of membership function in the prediction of the FLDs with experimental data is five and more bell-shape membership functions, but for decreasing the learning time the number five is chosen. It is found that the learning results of five membership functions have good agreement with the experimental data. The correlation of ANFIS output and the experimental data for ST12 sheet with three thicknesses of 0.7 *mm*, 1 *mm* and 1.25 *mm* and ST14 only with thickness of 0.7 *mm* are shown in Fig. 16. The best modeling results obtained by utilizing five membership functions for each input. Fig. 17 indicates the distribution of five bell membership functions of the input parameter of minor strain after hybrid learning in ANFIS. Fig. 18 represents distribution of five bell membership functions of the input parameters of minor strain and thickness for the experimental data of ST12 with different thicknesses. Moreover, the surface graph of major strain with any two inputs of minor strain and thickness for ST12 with three thicknesses of 0.7 *mm*, 1*mm* and 1.25 *mm* are shown in Fig. 19.

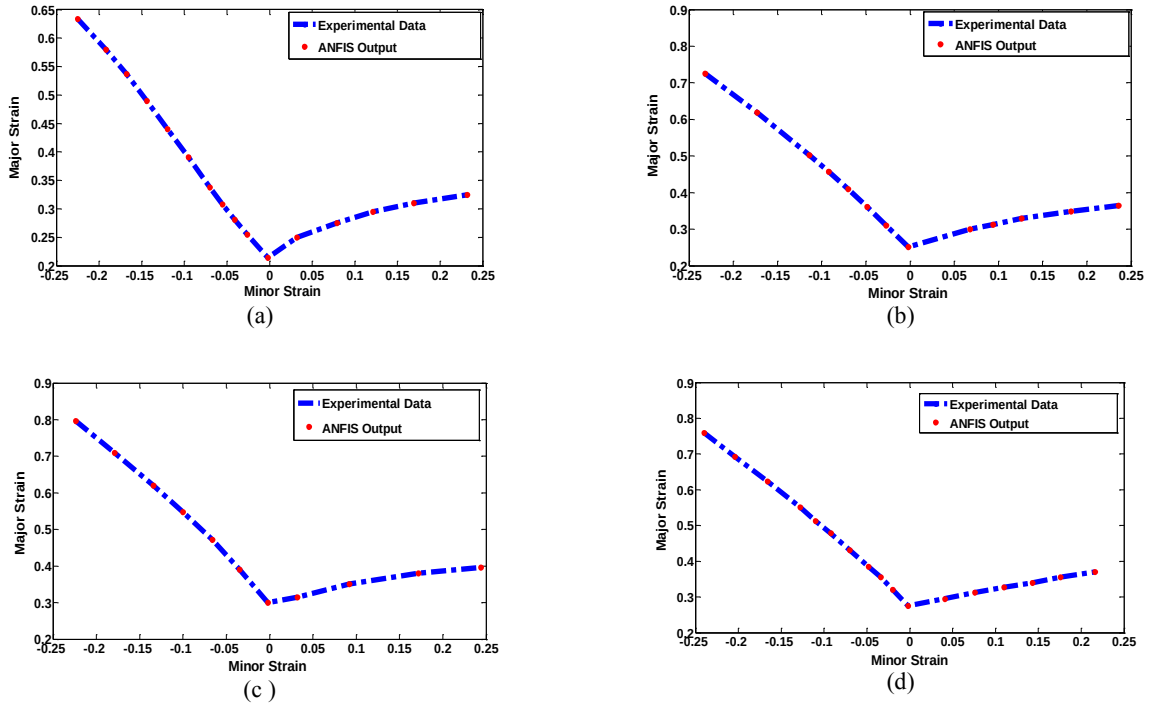

Fig.16
The prediction accuracy of ANFIS from experimental data: (a) St12-0.7 *mm*, (b) St12- 1 *mm*, (c) St12-1.25 *mm*, (d) St14- 0.7 *mm*.

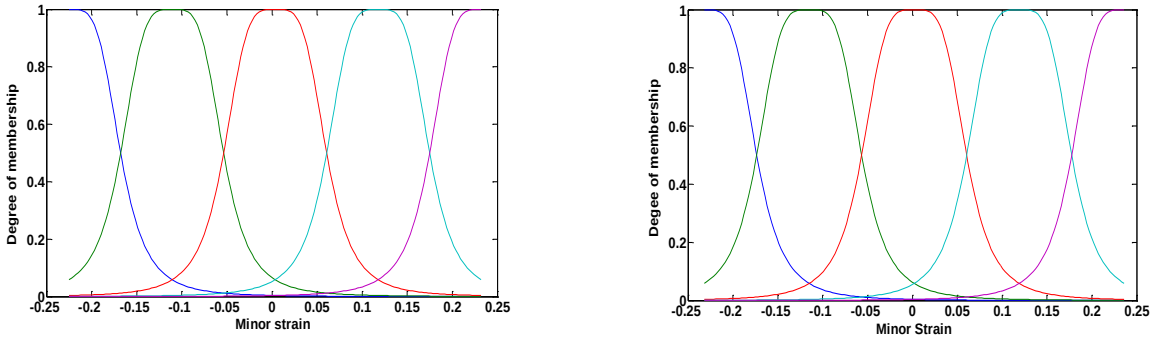

(a) (b)

Fig.17
Distribution of membership function for minor strain: (a) St12-0.7 *mm*, (b) St14-0.7 *mm*.

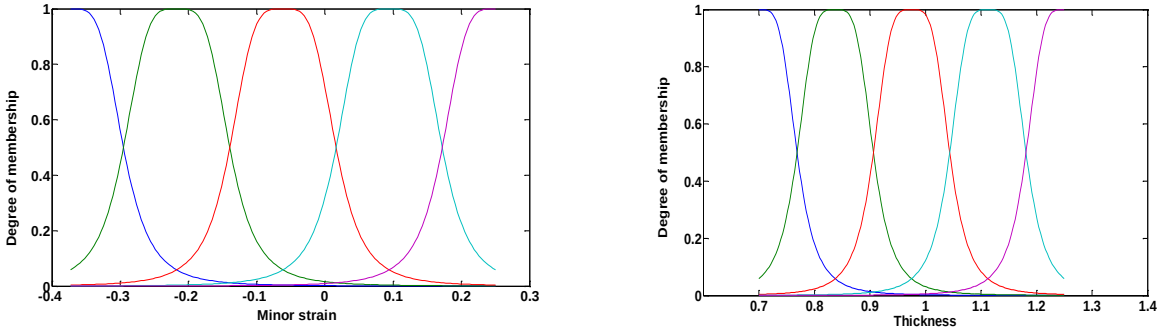

Fig.18
Distribution of membership function based on the experimental data of St12 for different thicknesses.

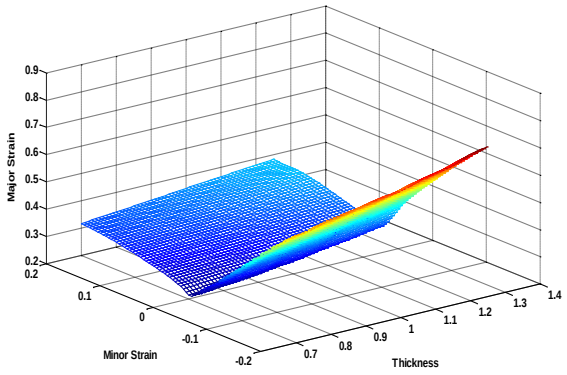

Fig.19
The surface plot from experimental data for the sheet of St12 with different thicknesses.

The values of principal strains at necking are measured by the solver explicit of ABAQUS software, as well. The material is modeled as elastic–plastic where the elasticity is taken to be isotropic and the plasticity is assumed as both isotropic and anisotropic conditions. According to experimental data for ST12 sheets of this literature and another experimental results [33, 34] with increasing thickness formability enhances. Based on experience, with increasing thickness the formability of ST14 sheet improves. Moreover, this study shows the effect of thickness on increasing of sheet metal formability on both left- and right-regions of the FLDs in both isotropic and anisotropic conditions, Fig. 12. After FE simulation of out-of-plane test for all sheets and obtaining numerical FLDs, databases of ANFIS are built and minor strain and thickness as input parameters and major strain as the output parameter are chosen.

The bell-shape membership function is adopted in the ANFIS training. The numbers of 5 to 30 membership function are investigated to seek the optimal number for prediction. It is found that the learning results for 25 membership functions have better agreement with FEM simulation. Fig. 20 depicts the distribution of 25 membership functions of the input parameter of minor strain after hybrid-learning in ANFIS. Fig. 21 represents the predicted and simulated results in the isotropic and anisotropic conditions for ST12 and ST14 sheets with similar thickness 0.7 *mm*. Figs. 22 and 23 show the obtained ANFIS mapping surfaces of input parameters, minor strain and thickness and output parameter of major strain for ST12 and ST14 sheets with three thicknesses of 0.7 *mm*, 1 *mm* and 1.25 *mm* in both isotropic and anisotropic conditions according to the training databases of FEM. These surfaces are useful to study the relations between each input parameter and major strain. The obtained results indicate that ANFIS outputs are in good agreement with experimental and FEM simulation, Figs. 16 and 21.

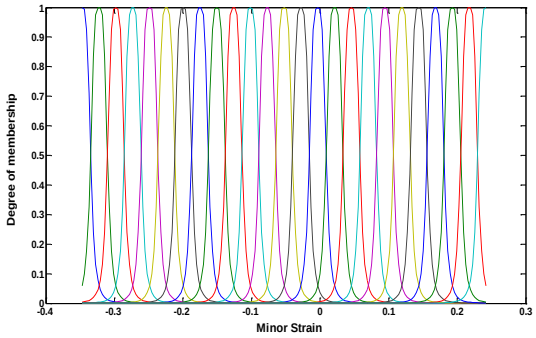

Fig.20
Distribution of membership function based on the FEM data of St12.

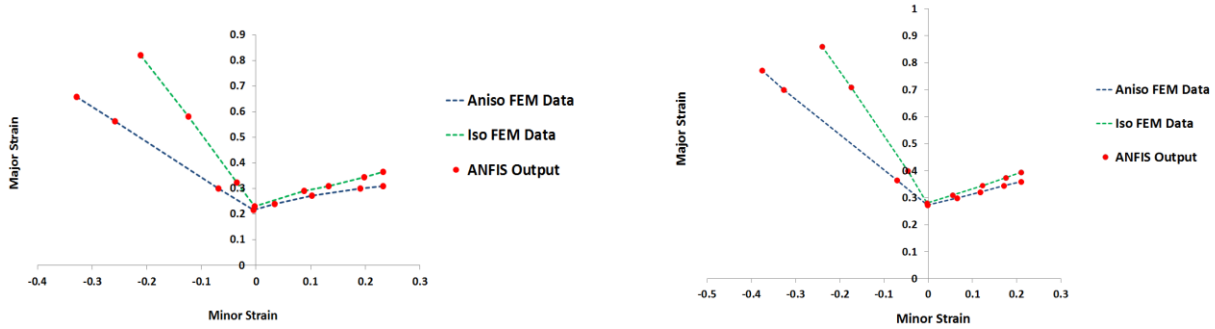

Fig.21
The prediction accuracy of ANFIS from simulation data in isotropic and anisotropic conditions: (a) St12-0.7 *mm*, (b) St14- 0.7 *mm*.

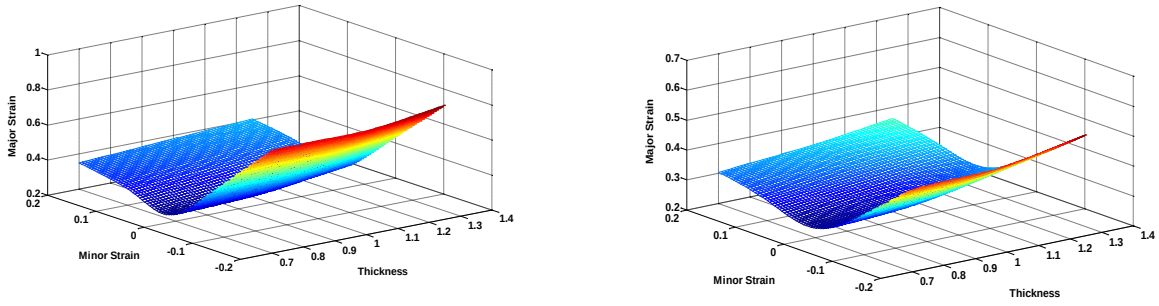

Fig.22
The surface plot from simulation data for the sheet of St12 with different thicknesses: (a) Isotropic, (b) Anisotropic.

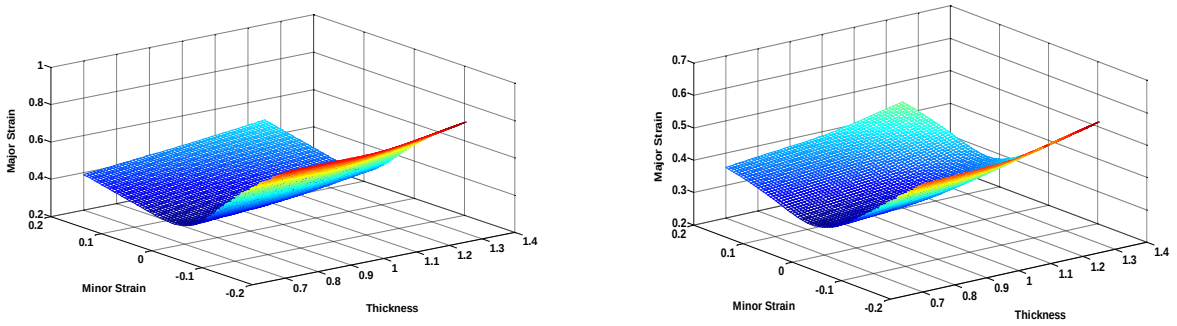

(a) (b)

Fig.23
The surface plot from simulation data for the sheet of St14 with different thicknesses: (a) Isotropic, (b) Anisotropic.

6 CONCLUSIONS

The non-traditional academic architecture adaptive network-based on fuzzy inference system was used to predict forming limit diagram. By employing the hybrid-learning algorithm, ANFIS could obtain the optimal distributed membership functions to describe the mapping relation in the input process parameters and output process property. This let the authors to elaborate on the reliability of the fuzzy inspired models for estimating the major and minor principal strains.

At first, the experimental procedure of out-of-plane test and the numerical simulation of out-of-plane stretching test by FE software Abaqus were completely scrutinized to determine the formability of low carbon steel sheets. In the simulation, localized necking of low carbon steel sheets was determined by tracing the thickness strain and its first and second derivatives versus time at the thinnest node. The effect of strain-hardening exponent and plastic strain ratio (*r*-value) along with the effect of thickness on FLDs were observed. The experimental results showed that by increasing the values of strain-hardening exponent and plastic anisotropy, the formability of the sheet increased. In addition, by increasing the thickness of the sheet, the forming limit strain increased. After obtaining the experimental and finite element results, the database of ANFIS model constructed by two input parameters, minor strain and thickness and major strain as output parameter. From soft computational point of view, it was observed that the fuzzy based identifiers were able to yield accurate results. On the other hand, obtained identification surfaces according to minor strain and thickness as input parameters and major strain as output parameter could predict the forming limit curve in the different thickness.

REFERENCES

[1] Keeler S.P., Backofen W.A., 1963, Plastic instability and fracture in sheets stretched over rigid punches, *ASM Trans* **56**: 25-48.
[2] Goodwin G.M., 1968, Application of strain analysis to sheet metal forming problems in the press shop, *SAE*, 680093.
[3] Hecker S.S., 1975, Simple technique for determining forming limit curves, *Sheet Metal Industries* **52**: 671-676.
[4] Marciniak Z., Kuczynski K., 1967, Limit strains in the processes of stretch forming, *International Journal of Mechanical Sciences* **9**: 609-620.
[5] Raghavan K.S., 1995, A simple technique to generate in-plane forming limit curves and selected applications, *Metallurgical and Materials Transactions* **26**: 2075-2084.
[6] Clift S.E., Hartley P., Sturgess C.E.N., Rowe G.W., 1990, Fracture prediction in plastic deformation processes, *International Journal of Mechanical Sciences* **32**: 1-17.
[7] Takuda H., Mori K., Hatta N., 1999, The application of some criteria for ductile fracture to the prediction of the forming limit of sheet metals, *Journal of Materials Processing Technology* **95**: 116-121.
[8] Takuda H., Mori K., Takakura N., Yamaguchi K., 2000, Finite element analysis of limit strains in biaxial stretching of sheet metals allowing for ductile fracture, *International Journal of Mechanical Sciences* **42**: 785-798.
[9] Ozturk F., Lee D., 2004, Analysis of forming limits using ductile fracture criteria, *Journal of Materials Processing Technology* **147**: 397-404.

[10] Brun B., Chambard A., Lai M., De Luca P., 1999, Actual and virtual testing techniques for a numerical definition of material, *Proceeding of Numisheet 99 Besançon*, France.
[11] Geiger M., Merklein M., 2003, Determination of forming limit diagrams-A new analysis method for characterization of materials formability, *Annals of the CIRP* **52**: 213-216.
[12] Petek A., Pepelnjak T., Kuzman K., 2005, An improved method for determining a forming limit diagram in the digital environment, *Journal of Mechanical Engineering* **51**: 330-345.
[13] Pepelnjak T., Petek A., Kuzman K., 2005, Analysis of the forming limit diagram in digital environment, *Advanced Material Research* **6/8**: 697-704.
[14] Friedman P.A., Pan J., 2000, Effects of plastic anisotropy and yield criteria on prediction of forming limit curves, *International Journal of Mechanical Sciences* **42**: 29-48.
[15] Huang H.M., Pan J., Tang S.C., 2000, Failure prediction in anisotropic sheet metals under forming operations with consideration of rotating principal stretch directions, *International Journal of Plasticity* **16**: 611-633.
[16] Cao J., Yao H., Karafillis A., Boyce M.C., 2000, Prediction of localized thinning in sheet metal using a general anisotropic yield criterion, *International Journal of Plasticity* **16**: 1105-1129.
[17] Wu P.D., Jain M., Savoie J., Mac Ewen S.R., Tugcu P., Neale K.W., 2003, Evaluation of anisotropic yield function for aluminum sheets, *International Journal of Plasticity* **19**: 121-138.
[18] Jang J.S.R., 1993, ANFIS: Adaptive-Network-Based Fuzzy Inference System, IEEE *Transactions on Systems, Man, and Cybernetics* **23**(3): 665-685.
[19] Lin J.C., Tai C.C., 1999, The application of neural networks in the prediction of sprint-back in an l-shaped bend, *International Journal of Advanced Manufacturing Technology* **15**: 163-170.
[20] Inamdar M., Narasimhan K., Maiti S.K., Singh U.P., 2000, Development of an artificial neural to predict spring back in air vee bending, *International Journal of Advanced Manufacturing Technology* **16**: 376-381.
[21] Kim D.H., Kim D.J., Kim B.M., 1999, The application of neural networks and statistical methods to process design in metal forming processes, *International Journal of Advanced Manufacturing Technology* **15**: 886-894.
[22] Cao J., Kinsey B., Solla S.A., 2000, Consistent and minimal springback using a stepped binder force trajectory and neural network control, *Journal of Engineering Materials and Technology* **122**: 113-118.
[23] Kazan R., Firat M., Tiryaki A.E., 2009, Prediction of spring back in wipe-bending process of sheet metal using neural network, *Materials and Design* **30**: 418-423.
[24] Wu C.Y., Hsu Y.C., 2002, Optimal shape design of an extrusion die using polynomial networks and genetic algorithms, *International Journal of Advanced Manufacturing Technology* **19**: 79-87.
[25] Yang G., Osakada K., Kurozawa T., 1993, Fuzzy inference model for flow stress of carbon steel, *The Japan Society for Technology of Plasticity* **34**(387): 422-427.
[26] Manabe K., Yoshihara S., Yan M., Nishimura H., 1995, Optimization of the variable BHF deep-drawing process by fuzzy model, *The Japan Society for Technology of Plasticity* **36** (416): 1015-1022.
[27] Ong S.K., Vin L.J.D.E., Nee A.Y.C., Kals H.J.J., 1997, Fuzzy set theory applied to bend sequencing for sheet metal bending, *Journal of Materials Processing Technology* **69**: 29-36.
[28] Baseri H., Bakhshi-Jooybari M., Rahmani B., 2011, Modeling of spring back in V-die bending process by using fuzzy learning back-propagation algorithm, *Expert Systems with Applications* **38**: 8894-8900.
[29] Lu Y.H., Yeh F.H., Li C.L., Wu M.T., 2005, Study of using ANFIS to the prediction in the bore-expanding process, *International Journal of Advanced Manufacturing Technology* **26**: 544-551.
[30] Lu Y.H., Yeh F.H., Li C.L., Wu M.T., Liu C.H., 2003, Study of ductile fracture and preform design of upsetting process using adaptive network fuzzy inference system, *Journal of Materials Processing Technology* **140**: 576-582.
[31] Hill R., 1948, A theory of yielding and plastic flow of anisotropic metals, *Proceedings of the Royal Society of London A* **193**: 281-297.
[32] Narayanasamy R., Narayanan C., 2006, Forming limit diagram for Indian interstitial free steels, *Materials and Design* **27**: 882-899.
[33] Triantafyllidis N., Samanta S.K., 1986, Bending effects on flow localization in metallic sheets, *Proceedings of the Royal Society of London* **406**: 205-226.
[34] JenabaliJahromi S.A., Nazarboland A., Mansouri E., Abbasi S., 2006, Investigation of formability of low carbon steel sheets by forming limit diagrams, *Iranian Journal of Science and Technology* **30**: 377-385.